Modeling the Effect of Anisotropy in Ultrasonic-Guided Wave Tomography

Madis Ratassepp, Jing Rao, *Member, IEEE*, Xudong Yu, and Zheng Fan

***Abstract*— Most of the existing ultrasonic-guided wave tomography approaches to map structural changes in plate-like waveguides are based on the assumption of an isotropic material model. However, there are many other engineering applications that are made of anisotropic materials and structures. Applying these techniques on such structures becomes complicated due to the anisotropic wave propagation behavior. The main challenge is to develop a suitable forward model that describes the wave propagation in such material, thereby enabling accurate reconstruction of the material properties. The present study proposes an anisotropic formulation of the acoustic forward model to map velocity variations induced by defects in anisotropic plates. The anisotropic behavior of the waves along the plate is simulated by implementing approximate anisotropic parameters. The velocity reconstruction is based on a full-waveform inversion algorithm, and its performance is investigated in the case of different degrees of anisotropy of the plate material and the defect. The results suggest that the method is highly suitable for imaging velocity changes due to defects. This is found to be the case when the defect has a similar anisotropic structure to the surrounding plate material. The validation experiment is performed on a multilayered composite plate with a circular defect of stiffness reduction using A_0 mode, showing a very good performance of the reconstruction algorithm.**

***Index Terms*— Acoustic forward model, anisotropy, full-waveform inversion (FWI), guided wave tomography (GWT).**

I. Introduction

GUIDED wave tomography (GWT) is an attractive method that enables the imaging of spatially varied material properties, by analyzing the ultrasonic signals captured by a transducer array around the inspection area. Thus, it is possible to quickly assess large inaccessible areas which are difficult and slow to inspect by conventional point-by-point measurement techniques. The majority of the research work on GWT has concentrated on isotropic materials: mainly metals. For example, several GWT algorithms have been developed for estimating the remnant thickness of corrosion patches in plate-like structures [1]–[7] and pipelines [8]–[10], which is a significant problem in the petrochemical and nuclear industries. However, there also exist many high-performance structural applications where anisotropic materials and structures are used. Composite pressure vessels [11], pipe elbows [12], and anisotropic stainless steel pipes [13] are some examples of such structures where routine inspection is required. Although guided wave testing has been proven to be a cost-effective and efficient nondestructive evaluation tool for anisotropic waveguides [14], [15], its utilization poses many difficulties. The ultrasonic wave behavior in these structures can be complicated by the directional dependence and complex defect geometry types, which make their analysis and application much more challenging [16], [17]. One of the key issues when using GWT for evaluating anisotropic waveguides is the proper modeling of velocity variations induced by anisotropy to obtain more accurate imaging results [18].

The reconstruction of the defects in GWT is based on the solution of an inverse problem that uses a forward model to predict a synthetic dataset for a given plate and defect shape. The shape of the defect is updated iteratively by minimizing the residuals between the true and synthetic measurements. Therefore, the performance of the method depends on the choice of a suitable forward model which should describe accurately the behavior of the wave propagation in the selected structure and it should be sensitive to changes in the properties to be reconstructed [19]. The use of 2-D acoustic models has been an attractive solution as they enable the reduction of the computational complexity and cost compared to full 3-D models, while reasonably capturing the behavior of guided waves. Previous studies have demonstrated that the acoustic forward model is appropriate to evaluate the thickness of the waveguides from the velocity [20]. It is also possible to reconstruct other parameters from the velocity, for example, the Young's modulus in a plate [21]. Another work investigated the imaging of flexural inhomogeneities in plates [22]. However, it should be noted that the material and the models describing the wave propagation in these studies were isotropic. It is more challenging to develop the acoustic forward model for an anisotropic medium where the wave

Manuscript received June 7, 2021; accepted September 19, 2021. Date of publication September 22, 2021; date of current version December 30, 2021. This work was supported in part by the European Regional Development Fund and the Program Mobilitas Pluss under Grant MOBTP46, in part by Estonian Research Council under Grant PRG737, and in part by the European Union's Horizon 2020 Research and Innovation Program under Grant 860104 Project Guided Waves for Structural Health Monitoring (GW4SHM). *(Corresponding author: Madis Ratassepp.)*

Madis Ratassepp is with the Department of Civil Engineering and Architecture, Tallinn University of Technology, 19086 Tallinn, Estonia (e-mail: madis.ratassepp@taltech.ee).

Jing Rao is with the School of Engineering and Information Technology, University of New South Wales, Canberra, ACT 2600, Australia.

Xudong Yu is with the School of Astronautics, Beihang University, Beijing 100191, China.

Zheng Fan is with the School of Mechanical and Aerospace Engineering, Nanyang Technological University, Singapore 639798.

Digital Object Identifier 10.1109/TUFFC.2021.3114432

propagation and its velocity are dependent on the stiffness of the material which itself is a complex quantity characterized by numerous constants [23].

Recently, Brath *et al.* [24], [25] have introduced an elliptically anisotropic acoustic forward model for the GWT to implement it in a pipe bend. It was demonstrated that the 3-D guided wave propagation in the bend could be modeled by a simple and efficient 2-D planar acoustic model. Anisotropic and inhomogeneous behavior of the wave velocity was described by a single parameter, which helped to achieve the travel-time-preserving condition for approximate isometric mapping. A similar model based on the assumption of elliptical anisotropy was used for the bulk wave imaging of defects in anisotropic-layered composites [26]. However, this assumption may not work for the cases where wavefronts exhibit more complicated forms than elliptical spreading. For example, nonelliptic propagation is inherent for guided waves in cross-ply-multilayered composite plates where the propagation energy is directed toward the main symmetry axes with larger stiffness [27]. To improve the acoustic modeling, we use an alternative parameterization of the wave field based on Thomsen-style parameters [28], [29]. These parameters give a simplified angular dependence of the wave velocities and enable the modeling of nonelliptic wavefronts. However, introducing more parameters in the model increases the ill-posedness of the inversion problem complicating the separation of individual parameters [30]–[32].

This work aims to investigate the applicability of the 2-D acoustic model in GWT for anisotropic plates. This model has been developed with the finite-difference (FD) discretization method, in which the velocity field is parameterized by the approximate Thomsen-style anisotropic parameters to make it artificially inhomogeneous and anisotropic. The model is used in the full-waveform inversion (FWI) algorithm to map the velocity variations caused by artificial stiffness defects modeled in multilayered composite plates with weak to moderate anisotropy. In this article, the low-frequency antisymmetric Lamb wave mode A_0 is used for the reconstruction of stiffness defects because the A_0 mode is known to be sensitive to stiffness variations [33].

This article starts with the description of the methods for acoustic forward modeling, its implementation for the guided wave problem and FWI in Section II. Numerical studies including finite element (FE) and acoustic modeling and the results of forward modeling and defect imaging are reported in Section III. In Section IV, an experimental study is presented, including measurement procedures and a validation experiment. Discussion of the effect of anisotropy of the plate and the defect on the accuracy of inversion and limitations in GWT follows in Section V. The conclusions are summarized in Section VI.

II. Methods

A. Acoustic Forward Model

Consider a composite plate as shown in Fig. 1. It is assumed that a guided wave propagating in a plate of varying stiffness

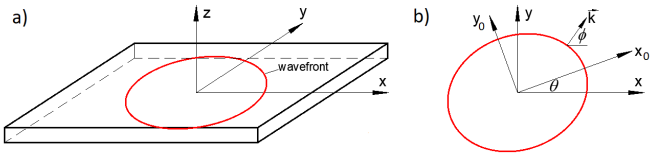

Fig. 1. (a) Acoustic model of guided wave propagation in a composite plate. (b) Top view of the wave-field with symmetry axis (x_0, y_0), tilt angle θ, wavenumber k, and phase angle ϕ.

will behave in the same way as an acoustic wave traveling in a 2-D medium with varying velocity. The acoustic wave is modeled in transversely isotropic media with a tilted symmetry axis and is described by a coupled system of second-order partial differential equations [34]

$$\begin{cases} \dfrac{1}{v_0^2}\dfrac{\partial^2 p}{\partial t^2} - (1+2\delta)Hp - H_0 p = (1+2\delta)Hq \\ \dfrac{1}{v_0^2}\dfrac{\partial^2 q}{\partial t^2} - 2(\epsilon-\delta)Hq = 2(\epsilon-\delta)Hp \end{cases} \tag{1}$$

where the differential operators H and H_0 are defined as

$$\begin{cases} H = \cos^2\theta\dfrac{\partial^2}{\partial x^2} + \sin^2\theta\dfrac{\partial^2}{\partial y^2} - \sin\ 2\theta\dfrac{\partial^2}{\partial x\partial y} \\ H_0 = \sin^2\theta\dfrac{\partial^2}{\partial x^2} + \cos^2\theta\dfrac{\partial^2}{\partial y^2} + \sin\ 2\theta\dfrac{\partial^2}{\partial x\partial y}. \end{cases} \tag{2}$$

Expression p is the pressure wavefield, q is an auxiliary wavefield, and v_0 is the pressure wave velocity along the symmetry axis. The values ϵ and δ are anisotropic parameters defined by Thomsen [28], and θ is the angle of symmetry axis with respect to the x-axis. If $\epsilon = \delta$, the second equation in the system of (1) vanishes and the model becomes elliptically anisotropic. In case of $\epsilon = \delta = \theta = 0$ the (1) reduces to the second-order acoustic isotropic wave equation. The cross-derivative terms in both differential operators H and H_0 are responsible for the rotation of the symmetry axis.

It should be noted that these equations are much simpler than their elastic counterparts by minimizing the effect from shear waves, and yet yield exceptionally accurate descriptions of the traveltime and geometrical amplitude, or wavefront spreading [35]. Furthermore, the kinematic behavior of propagating waves in the case of a known symmetry tilt angle can be characterized by just three model parameters: v_0, ϵ, and δ. It should be noted that the solution of (1) becomes unstable when $\epsilon < \delta$. This is due to unstable shear waves which are regarded as artifacts in the framework of acoustic modeling [36]. This instability can be reduced in the case of frequency-domain modeling with absorbing boundary conditions [37].

B. Anisotropic Parameters for Plate Guided Waves

In acoustic media, velocity and anisotropic parameters can be explicitly derived from the stiffness constants of the medium. However, for the plate case such simple relations do not exist. In the case of weak anisotropy of the medium, the acoustic velocity model can be fit with the guided wave model using approximated Thomsen parameters [28].

These parameters can be obtained using the first-order terms of the linearized phase velocity v_{ϕ_0} at a few discrete phase angles as follows:

$$\epsilon = \frac{v_{90} - v_0}{v_0}$$
$$\delta = 4\left[\frac{v_{45}}{v_0} - 1\right] - \epsilon \tag{3}$$

where v_0 is the phase velocity along the symmetry axis at $\phi_0 = 0$. The velocities v_{45} and v_{90} are the phase velocities at the phase angle $\phi_0 = 45°$ and 90°, respectively. Parameter ϵ shows the relative velocity difference along the symmetry axes of the problem, while δ describes the velocity variation at intermediate phase angles.

C. Full-Waveform Inversion

The FWI is a local optimization process. It uses a forward solver to predict the scattering of a guided wave through the stiffness defects, and an iterative inversion model to reconstruct the defect in terms of velocity. At each iteration, numerical modeling is carried out with the aim of least-squared minimization of the residual data between the data predicted by the model and the data observed from simulations or experiments. The FWI makes use of the full information of the wave-field, thus enabling a more accurate inversion result to be achieved that is also advantageous in imaging irregularly shaped and multiple defects [7], [20]. Here, the theory is briefly revisited. A review of FWI and its application is provided in [38].

In this article, the forward problem is solved numerically by transforming the equation system (1) into the frequency domain and discretizing with the FD method using the mixed-grid approach [37]. After discretization, the equation can be presented in matrix form as

$$AP = S \tag{4}$$

where A denotes the impedance matrix, the coefficients that depend on the modeled frequency and the model parameters, and the matrices $P = [p_1, p_2, \ldots, p_n]$ and $S = [s_1, s_2, \ldots, s_n]$ contain the predicted pressure wavefields and sources, respectively, stored as column vectors. The linear equation system (4) can be solved efficiently by reusing the LU factorized matrix A for a multiple source problem [39] given by the following expression:

$$LU[p_1 p_2, \ldots, p_n] = [s_1 s_2, \ldots, s_n] \tag{5}$$

where n is the number of sources.

The minimization is carried out using the Seiscope optimization toolbox [40]. Its basic principle is to solve a linearized least-squares problem where the misfit function $f(m)$ between the forward modeled $p_s(m, \omega)$ and observed wavefields $d_s(\omega)$ is minimized and expressed as

$$\min_m f(m) = \frac{1}{2}\sum_{s=1}^{n} ||p_s(m, \omega) - d_s(\omega)|| + T(m, \omega) \tag{6}$$

where m is the inverted model parameter, ω is the angular frequency, s denotes the dataset in n, and $T(m)$ is a regularization term (not implemented in this work). The model update m_k along its descent direction Δm_k is obtained from the recurrence

$$m_{k+1} = m_k + \alpha_k \Delta m_k \tag{7}$$

where α_k is a scalar step length. The descent direction of the model Δm_k is computed with a nonlinear conjugate gradient method and is given as a linear combination of the opposite of the gradient and the descent direction computed at the previous iteration

$$\begin{cases} \Delta m_0 = -He_0^{-1}(m_0)\nabla f(m_0) \\ \Delta m_k = -He_k^{-1}(m_k)\nabla f(m_k) + \beta_k \Delta x_{k-1}, \quad k > 1 \end{cases} \tag{8}$$

where $He_k(m_k)$ is a Hessian operator, $\nabla f(m_k)$ is the gradient function, and β_k is a scalar search parameter.

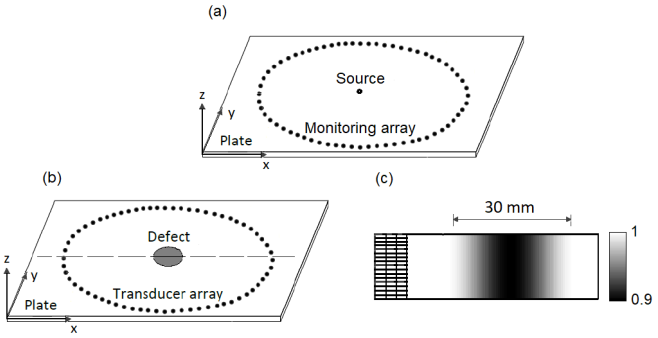

Fig. 2. (a) Plate setup with a central source and a circular monitoring array surrounding it. (b) Plate setup with a central stiffness defect and a circular transducer array surrounding it. (c) Cross section of the meshed plate with a through-thickness defect.

TABLE I
STIFFNESS CONSTANTS (IN GIGAPASCAL) OF THE SE84LV PREPREG PLY USED IN THE PRESENT STUDY; THE MASS DENSITY IS 1540 Kg/m^3; THE PLY THICKNESS IS 0.15 mm

C_{11}	C_{12}	C_{13}	C_{22}	C_{23}	C_{33}	C_{44}	C_{55}	C_{66}
107.8	4.51	4.51	10.31	4.24	10.31	3.04	4.45	4.45

III. NUMERICAL STUDY

A. FE Modeling

The software Abaqus Explicit was used for the wave propagation simulations [41]. Two separate configurations were considered for modeling. In the first case, the performance of the forward modeling was investigated by exciting the waves at the center of the composite plate and monitoring them with a surrounding circular array, shown in Fig. 2(a). The aim is to compare the polar distribution of the propagating wavefronts obtained from FE and acoustic modeling. The second configuration is presented in Fig. 2(b), where the imaging problem is illustrated. In this model, transducers were placed around the circular stiffness defect to transmit and receive waves through the plate. The array in both cases was 200 mm in diameter and 40 transducers were used in the array.

The composite plates were modeled with 16 plies made of carbon fiber/epoxy with material properties given in Table I [42]. In the FE model, each ply was modeled individually and the plies were tied together at the interfaces

to build the laminate. The reference coordinate system used to define fibrous materials was set such that the fibers lay along the x-axis and the layer interfaces were normal to the z-axis. The plate was meshed by eight-node brick elements (C3D8R), with a size of 0.4 mm along the length and width directions and 0.15 mm along the thickness direction, to ensure at least one element for each ply thickness. Three different stacking sequences of the plies were considered to investigate the degree of anisotropy in the performance of GWT. The sequence $[0/45/90/-45]_{2S}$ represents the plate where the wave propagation is nearly isotropic and is hereinafter referred to as quasi-isotropic. In cross-ply laminate $[0/90]_8$, the wave energy tends to propagate along the principal axes and in the unidirectional plate $[0]_{16}$, the waves propagation is fastest and strongest along the fiber direction. Absorbing layers were applied to minimize reflections from the edges of the plate [43].

One of the most common type of damage encountered in composite structures is the reduction of local stiffness which can be the result of an impact, fracture or exessive thermal loading. It has been found that this may affect the anisotropy of the damaged material [44]. The aim here is to study these effects on simple artificial defects. The defect is shown in Fig. 2(c) and was modeled as an axisymmetric defect with reduced stiffness or with changing material anisotropy. In the case of the stiffness defect, all the reduced stiffness constants of each element at every layer were assumed to be similar. Along the xy-plane the stiffness was changed smoothly according to Hann-shape variation [21] with a maximum loss of 10% at the center of the defect. In the case of an anisotropic defect the stiffness constants of the elements are not changed but the orientation of the fiber direction of the elements at every layer through the thickness was smoothly changed to obtain the desired anisotropy at the defect center. The description of the defect used in the modeling for experimental comparison is given in Section IV.

A five-cycle Hann-windowed tone-burst signal at 50 kHz was simulated as the input signal. For a given source point in the array, the A_0 mode was generated by applying an out-of-plane force and the wavefields were measured by the rest of the receivers of the array. This was repeated for all the source–receive combinations resulting in a 40×39 signal matrix. These signals were transformed into a frequency domain and the required frequency components for the inversion were extracted and calibrated [7].

B. Acoustic Modeling

To simulate the plate-like guided wave propagation in the acoustic model, prior knowledge about the guided wave mode propagation behavior in the actual composite plate is required. The slowness curves for the A_0 mode at 50 kHz are shown in Fig. 3(a) for the studied laminates. The results were obtained from the wave simulations of FE modeling. The phase angle $\phi = 0$ corresponds to the x-direction of the composite plate. It can be seen that the anisotropic wave propagation behavior is inherent for all composite lay-up cases. In the case of the nearly quasi-isotropic plate $[0/45/90/-45]_{2S}$, the slowness profile is slightly elliptical and asymmetrical and its apparent

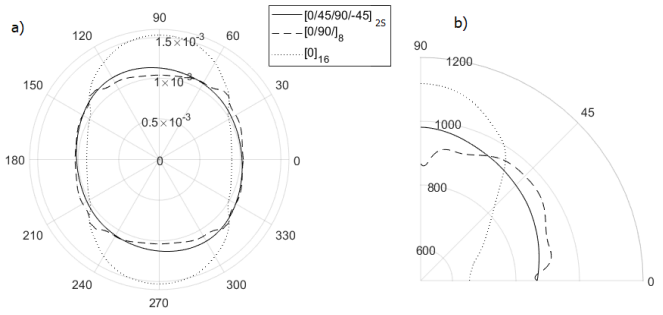

Fig. 3. Characteristic wave curves for A_0 mode at 50 kHz for different composite lay-ups: (a) slowness $s(\phi) = k(\phi)/\omega$; (b) phase velocity $c_{\text{ph}}(\phi)$.

TABLE II
WAVE SIMULATION PARAMETERS IN ACOUSTIC MODELING

Composite lay-up	θ (°)	v_0 (m/s)	ϵ	δ
$[0/45/90/\text{-}45]_{2S}$	108	868	0.13	0.13
$[0/90]_8$	45	866	0	0.45
$[0]_{16}$	90	654	0.71	0.35

symmetry axes are rotated with respect to the x-axis. This comes from the fact that the distribution of the stiffness of the plate is asymmetrical and the wavefield of the A_0 mode is sensitive to the direction of fibers close to the surface layers. The slowness profile of the cross-ply plate $[0/90]_8$ tends to a rectangular shape, having the largest values of slowness at 45° from the symmetry axes. The wave propagation is very anisotropic in the unidirectional composite plate $[0]_{16}$, having a slowness profile which is highly elongated along 90°. The respective velocity curves obtained in the first quarter of the coordinate system are shown in Fig. 3(b). The phase angle $\phi = 0$ was set along the selected symmetry axis with the smallest phase velocity. The curves show that the phase velocity varies with the phase angle for all plate cases. The resulting parameters for the acoustic modeling are shown in Table II: tilt angle θ, phase velocity along the symmetry axes x_0, and Thomsen parameters ϵ and δ. An alternative choice of the main symmetry axis can also be along the faster direction, which has the result that some Thomsen parameters become negative.

The simulations in the acoustic domain were performed with the FD method and the calculation domain consisted of 250×250 grid points and was sampled with a grid spacing of 1 mm. All the starting models used for the inversion were homogeneous background models of v_0, ϵ, and δ, except for the case of the unidirectional composite plate where $\epsilon > \delta$, which may excite an undesired shear wavefield. In this case at the source point a small, smoothly tapered circular region with $\delta = \epsilon$ was set to cancel out the shear wave excitation [45]. This introduces only a small kinematic error in directions deviating from the horizontal or vertical direction.

C. Forward Simulation Results

For the simulation, we consider wave propagation in three different composite plates; the properties are summarized

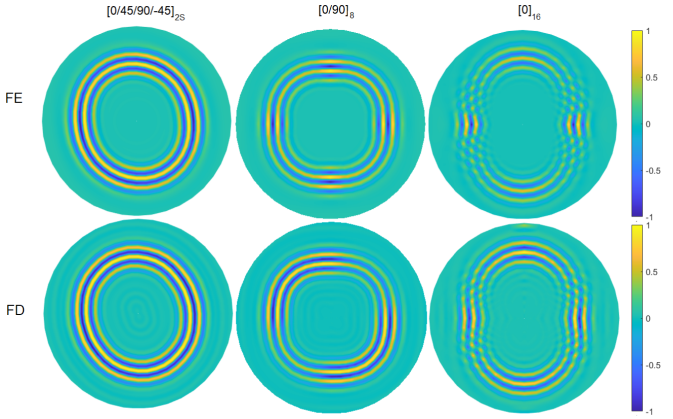

Fig. 4. Forward modeling results of the A_0 mode excited at 50 kHz obtained from FE and FD simulations for different composite lay-ups.

in Table I. The source is in the center of the circular receiver array with a diameter of 200 mm. Fig. 4 presents a comparison of the time-domain snapshots of the generated wave fields of the A_0 mode propagation at 50 kHz obtained from FE and FD simulations, respectively. The horizontal axis matches with the x-axis. The radial coordinate of the polar plot denotes the propagation time and the color of the contour shows the amplitude of the normal displacement of the plate. Good agreement can be seen between the wavefronts obtained from the methods used for all plate cases, whatever the direction of propagation. However, some mismatch between the amplitudes of the simulated waveforms can be observed. For the cross-ply laminate, the wave energy tends to propagate along the principal symmetry axes in the FE model while in the FD model the energy distribution is nonsymmetric and is focused along 135° and 315°. In the case of the unidirectional composite plate, the wave energy strongly concentrates along the fiber direction in the FE result but is more equally distributed along all directions in the FD result. This indicates that the forward modeling becomes less accurate when the anisotropy of the medium increases. In general, this numerical example demonstrates the suitability of the introduced 2-D acoustic model to predict waveforms of guided waves in composite plates with weak and moderate anisotropy.

D. Inversion Results

1) Effect of Forward Model (Isotropic Versus Anisotropic Model): In the first case, we compare the reconstruction results of the defects in composite plates using either an isotropic or an anisotropic forward model in FWI. Reconstructed velocity maps were obtained by inverting the FE data at 50 kHz by starting from the homogeneous background velocity along the symmetry axis and Thomsen parameter models and using 40 iterations for the inversion. In the isotropic model, the Thomsen parameters of the background were set to zero. A 30-mm wide defect with stiffness loss in the plate center is imaged in Fig. 5 using the anisotropic forward model. It can be seen that the defect is well reconstructed retaining its circular shape for all plate cases. The inversion results using different forward models are compared in Fig. 6. It can

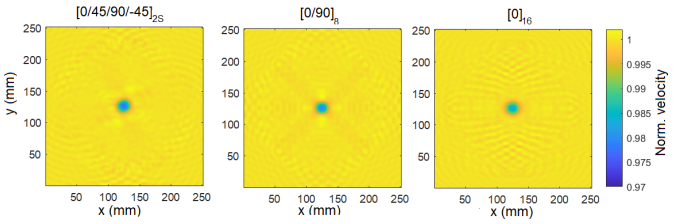

Fig. 5. FWI results with an anisotropic forward model using A_0 mode at 50 kHz: normalized velocity v_0 maps for different composite lay-ups with central 30 mm Hann-shaped stiffness defect with maximum loss in stiffness constants of 10%.

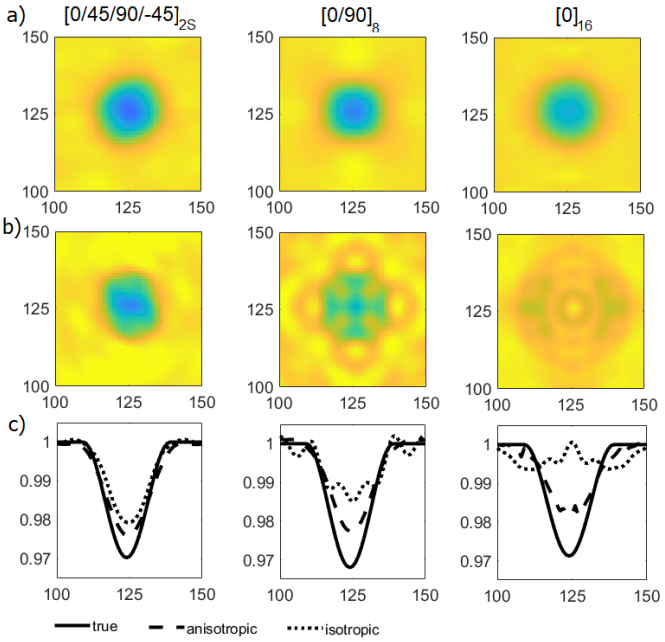

Fig. 6. Comparison of the reconstructed velocity maps using different forward modeling: (a) anisotropic forward model, (b) isotropic forward model, and (c) cross section of the defect at $y = 125$ mm.

be clearly seen that the anisotropic forward model provides much more accurate velocity reconstructions compared to the isotropic forward model. The shape of the defect in the quasi-isotropic plate is distorted with the isotropic model and it completely fails to image defects for plates with an increasing material anisotropy. This example clearly demonstrates the need to consider anisotropy in the forward model for accurate inversion.

2) Effect of Defect Size: Second, we apply FWI with the anisotropic forward model to reconstruct the stiffness defects with varying diameters of 15 mm ($\simeq 0.9\lambda$), 30 mm ($\simeq 1.8\lambda$), 60 mm ($\simeq 3.5\lambda$) (λ - wavelength), and fixed maximum stiffness loss in the plate center. Fig. 7 presents the comparisons of the cross section of the reconstructed velocity and the true velocity for defects with varying surface sizes. It can be seen that the largest defect is very well reconstructed in the quasi-isotropic plate. The accuracy of estimating the minimum velocity and the ability to resolve its width deteriorates with decreasing defect size. Also, the accuracy degrades with increasing anisotropy of the plate material, which can be related to the decreasing accuracy of the forward modeling of more

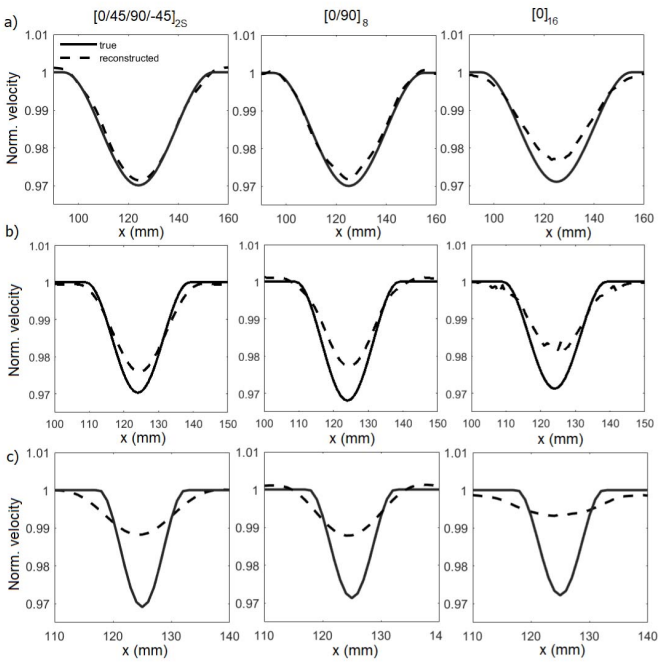

Fig. 7. FWI results with A_0 mode at 50 kHz: cross section of the normalized velocity v_0 profile of the defect at the plate center for different composite lay-ups with varying surface diameter of (a) 60 mm, (b) 30 mm, and (c) 15 mm.

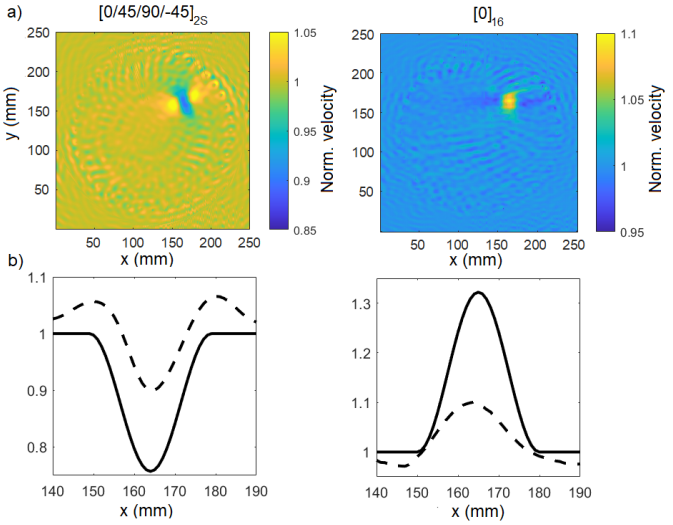

Fig. 8. FWI results with A_0 mode at 50 kHz: (a) normalized velocity v_0 maps for different composite lay-ups with noncentral 30 mm Hann-shaped anisotropic stiffness defect. (b) Cross section of the defect at $y = 165$ mm.

anisotropic material demonstrated in Section III-D.1. Ideally, in tomographic imaging velocity variation down to $\lambda/2$ can be reconstructed when the forward model matches exactly the real physical model. However, poorer resolution and accuracy can be expected due to the acoustic forward model, which does not account for all the wave physics of guided wave propagation in a plate. This finding is a similar to previous studies with isotropic materials, where velocity variations around 2λ can be reconstructed using acoustic forward models [19], [20].

3) Anisotropic Effect in a Defect: The last case considers the velocity reconstruction of anisotropic defects. An example is delamination in a composite laminate. The delamination divides the region into several waveguides which have respective anisotropic properties according to the lay-up of the sublaminate, which may differ from the properties of the surrounding plate. In previous cases, only the stiffness of the defect was slightly reduced, which does not vary significantly the Thomsen parameters in the defect area compared to the background values. Here we investigate artificial defects in which the Thomsen parameters are changed considerably. The studied defects are 30 mm in width and off-set from center by 40 mm in both coordinate directions. The first defect is considered in the quasi-isotropic plate. The orientation of the fiber direction inside the defect is smoothly changed from the fiber direction of the surrounding plate such that in the center of the defect it has the lay-up of a unidirectional lay-up as $[18]_{16}$, which means that the fibers of all layers are along 18°. Its corresponding parameters for the acoustic model are $\theta = 108°$, $v_0 = 654$ m/s, $\epsilon = 0.71$, and $\delta = 0.35$. The parameters for a background plate model are given in Table II. The second defect is modeled in the unidirectional plate having the lay-up in the center as $[-18/27/72/-63]_{2S}$ and its corresponding parameters in the acoustic model are $\theta = 90°$, $v_0 = 868$ m/s, $\epsilon = 0.13$, and $\delta = 0.13$. It represents the quasi-isotropic lay-up configuration which is rotated by $-18°$ compared to the x-axis. The nontrivial rotation angle of the defect in both plate models is necessary to match the symmetry axes of the defect and the surrounding plate in acoustic modeling. The imaging results are shown in Fig. 8(a) and we can see that defects are detectable; however, their shapes become more irregular and the image around the defect contains artifacts. Comparisons between the reconstructed velocity and the true velocity are shown in Fig. 8(b) and it can be seen that the accuracy of the reconstruction compared to previous cases decreases. This indicates that it is more challenging to image defects with a strong anisotropy, and the reasons are discussed in Section V.

IV. Experimental Study

A. Specimen and Measurements

The experimental setup composed of a composite plate of 500 mm × 500 mm × 2.4 mm made of 16 layers with the lay-up of $[0/45/90/-45]_{2S}$. The properties of each lamina were the same as those for the simulations, as shown in Table I. Initially, three separate ply laminates with lay-ups $[0/45/90/-45]$, $[0/45/90/-45]_S$ and $[-45/90/45/0]$ were prepared and cured in an autoclave. A circular hole with a diameter of 30 mm was cut into the center of the second laminate. The hole was filled with a resin Epolam 2051 + 3M glass microballoons (with Young's modulus 2.9 GPa, assumed Poisson's ratio 0.33, and density 810 kg/m^3) and the three laminates were bonded together with an adhesive film and cured in the oven under vacuum pressure. This represents the plate with a defect area with a reduced stiffness in the plate center, as shown in Fig. 9(a).

The experimental setup is shown in Fig. 9(b). Ultrasound tomography measurements were performed with a 40 element

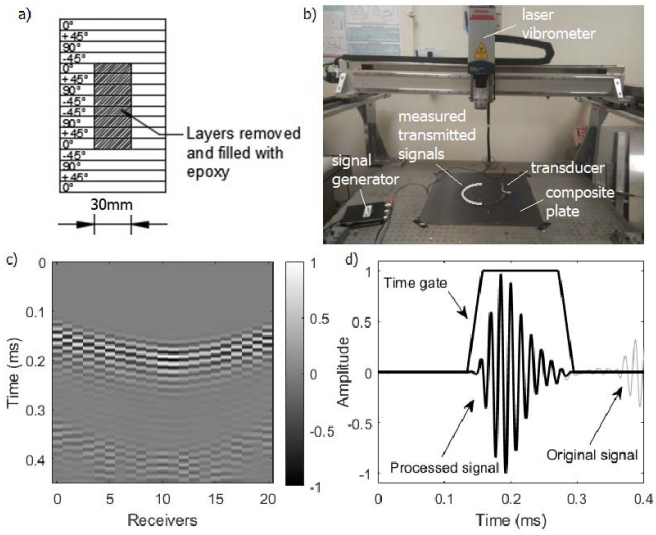

Fig. 9. Experimental measurements: (a) cross section of the composite plate with a stiffness defect. (b) Setup to measure ultrasound propagation in a composite plate. (c) Contour plot of the measured out-of-plane displacement of 21 measured signals. (d) Experimental time trace from the seventh receiver and the signal after time gating.

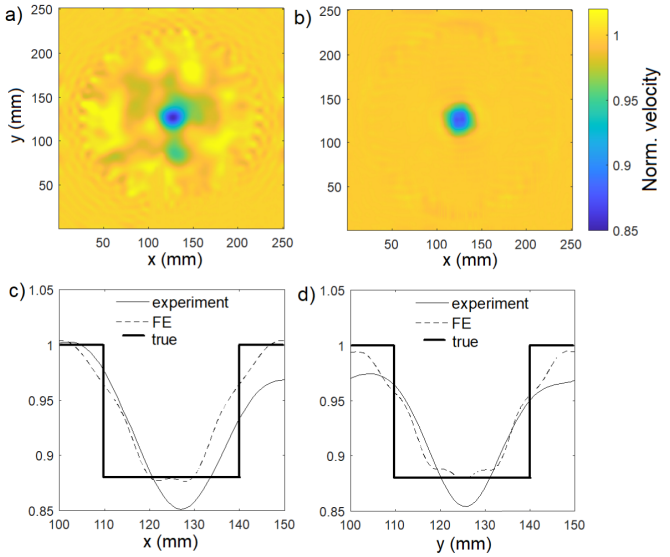

Fig. 10. Normalized velocity obtained with FWI using the A_0 mode at 50 kHz: (a) experiment. (b) FE. (c) Horizontal cross section. (d) Vertical cross section.

array with a diameter of 200 mm. A piezoelectric transducer (Doppler, Guangzhou, China) with a center frequency of 70 kHz coupled to the composite plate was used to excite the A_0 mode at one position. A PolytecOFV-505 laser vibrometer was used to measure the displacement normal to the surface. In each measurement, a five-cycle Hann-windowed tone-burst signal centered at 60 kHz was generated by a Tiepie Handyscope HS3. The measurements were taken on half of the circle with 21 measured points in the transmission zone. A contour plot of the typical measured out-of-plane displacement signals is shown in Fig. 9(c). A gating function shown in Fig. 9(d) was applied to remove unwanted components and the first arrival wavepacket was obtained. This process was repeated for 40 excitation points to build up a matrix of 40×21 signals.

B. Validation

Reconstructed velocity maps were obtained by inverting the data at 50 kHz by starting from the homogeneous background velocity along the symmetry axis and Thomsen parameter models, and using 40 iterations for the inversion. The normalized velocity reconstructed from the experimental measurements and FE modeling is shown in Fig. 10(a) and (b), respectively. It can be seen that the velocity drops in the area of the defect at the plate center. The images of the defects obtained by different approaches are slightly different. In the experiment the defect is circular, while in FE modeling it is slightly elliptical elongated along the y-axis. Comparisons between the reconstructed velocity and the true velocity along the cross section of the plates are shown in Fig. 10(c) and (d). It can be seen that the velocity drop is a bit overestimated in the experiment and very well reconstructed from the FE data. It is believed that the reason for such overestimation may be the lower stiffness and smaller thickness of the plate in the defect area, likely due to the shrinkage during curing. It should also be noted that this defect is more complicated compared to the one used in FE with smoothly changing material properties. The defect splits the waveguide into three parts with a layer in the center with much lower acoustic impedance. This would produce energy trapping and additional scattered wavefields, which are not encountered in the acoustic model [46].

V. Discussion

The results of this study demonstrated that a simple and efficient acoustic forward model can be used to map high resolution velocity images in anisotropic plate-like waveguides by FWI. The approach uses Thomsen parameters which can effectively link the true guided wave velocities with the velocities of the acoustic model. This is advantageous in applications where Thomsen parameters can be easily determined and velocity information used for the defect characterization. However, it was shown that the reconstruction accuracy decreased with increasing anisotropy of the background material and the defect.

In the first case, one of the reasons was that the amplitude modeling in forward modeling became less accurate while the phase was accurately predicted. One way to reduce this error is to consider only the phase information in the misfit minimization criteria or to use heuristic amplitude corrections in the measured data [38]. Another approach could be to modify the pressure source with appropriate directivity weights to achieve the correct waveform amplitudes [47]. However, it should be noted that this reconstruction error cannot be fully eliminated as the model is based on the acoustic assumption rather than on a full 3-D model and in addition the model is intended for weakly anisotropic media.

Second, it was found that the accuracy of the velocity reconstruction of the defects was considerably reduced if their Thomsen parameters diverged significantly from the background parameters. Such loss in accuracy is due to the coupling between the parameters involved in the inversion

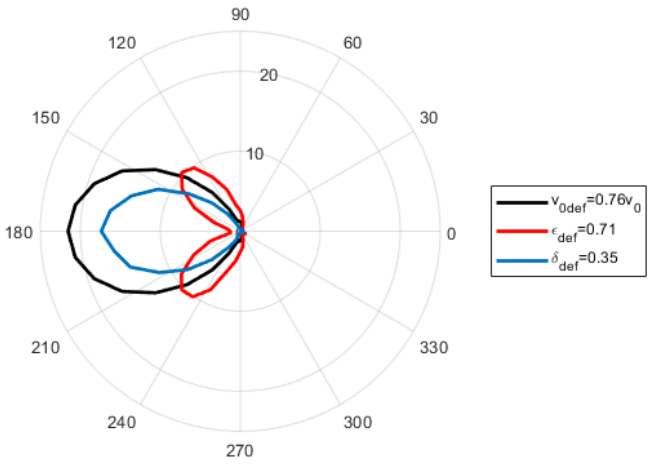

Fig. 11. Scattering patterns of different perturbation parameters at 50 kHz, acoustic parameters of the background medium $v_0 = 868$ m/s, $\epsilon = 0.13$, $\delta = 0.13$.

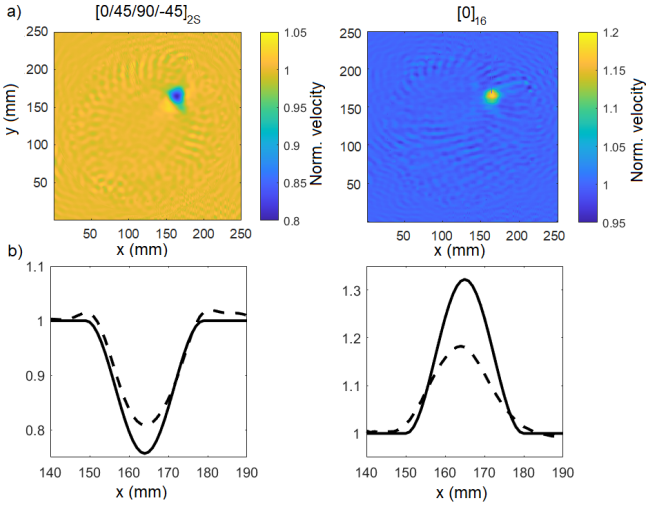

Fig. 12. FWI results with A_0 mode at 50 kHz: (a) normalized velocity v_0 maps for different composite layups with noncentral 30 mm Hann-shaped anisotropic stiffness defect with true starting models of ϵ and δ. (b) Cross section of the defect at $y = 165$ mm.

which increases the ill-posedness of the inversion because the sensitivity of the inversion can change significantly from one parameter to next parameter [38]. Fig. 11 shows the scattering patterns obtained from the different individual perturbation parameters (v_0, ϵ, and δ) with Hann-shaped variation in the acoustic model. The parameters of the defect in quasi-isotropic plate from Section III-D.3 were used in the calculation with the source located at 0° in the array. It can be seen that the scattered pressure fields are mainly induced to the forward direction and are dominated by the scattering from velocity perturbation (the amplitudes of the fields of ϵ, and δ are multiplied by 50 for comparison). Overlap in the scattering patterns means that the fields from different parameters are not separable. This results in a similar gradient update in the inversion for different parameters, making it difficult to distinguish the individual parameters. A potential solution to this problem could be to implement the multiparameter inversion, which could also help to recover the Thomsen parameters. However, this requires the development of a more sophisticated inversion method that can manage the different scale and sensitivity of the inversion parameters [48], which is beyond the current study. To demonstrate the potential improvement in the inversion accuracy if some parameters of the defect are better defined, we show the reconstruction of the velocity of the anisotropic defect in quasi-isotropic plate and unidirectional plate from Section III-D.3. The starting models of Thomsen parameters include the true variation due to defects. The imaging results with cross sections of the defects are shown in Fig. 12 and we can see that the reconstruction improves compared to the results shown in Fig. 8.

Some limitations in this study should be mentioned. Given that the imaging errors of the method increase with the increasing anisotropy of the model, this indicates that the approach may be less suitable for applications where the wave propagation is very anisotropic. The velocity of the S_0 mode is more affected by the in-plane stiffness and orientation of the layers than the A_0 mode and can be very anisotropic in cross-ply and unidirectional composite plates [49]. In this work, we demonstrated that the inversion is successful for a moderately anisotropic plate with specific Thomsen parameters. However, these anisotropic parameters may vary for different composite lay-up configurations and the impact of this on the inversion performance is unknown and should be further investigated.

The model assumes that the symmetry axes of the material are known *a priori*. However, in some cases, their orientation is unknown or is difficult to determine. In this case there is a risk that the chosen orientations do not exactly match with the material axes, which can impact the accuracy of the inversion. For example, in some metals such as duplex stainless steel the texture can be characterized by the presence of grain alignments oriented in a particular way [50], which causes local anisotropy in the material and complicates the selection of symmetry axes. The model also assumes that the wave propagation in the plate has two symmetry planes. This condition may be not met for the flexural mode in unbalanced laminates and quasi-isotropic laminates having a small number of layers. One way to assess this is to evaluate the symmetry of the flexural stiffness of the plate as the wave velocity is proportional to the stiffness [51].

The study investigated very simple defects in multilayered composite plates. In reality, defects such as those induced by impact events can have a much more complicated stiffness loss distribution across the plate thickness. In addition to this, the previously mentioned change in anisotropy and orientation of symmetry axes may also be present in the damage. Therefore, the proposed method can provide only an estimate of averaged through-thickness stiffness loss about the defect. Further investigations are required to understand the effects from different defect parameters to reduce the uncertaintes in the inversion problem.

VI. Conclusion

In this article, an efficient GWT method is developed for characterizing defects in anisotropic plates. It includes a forward model which enables the description of 3-D

elastic-guided wave propagation in an anisotropic plate by means of an equivalent 2-D anisotropic acoustic model, and an inverse model to update the velocity map. The equivalence is established based on implementing approximate anisotropic Thomsen parameters that describe the angular variability of the velocity in the plate. The GWT has been applied to the simulated and experimentally measured data of a through-thickness stiffness loss and an embedded stiffness flaw in a multilayered composite plate, showing good performance in determining the location, shape, and size of the defects. The most accurate inversion results have been obtained for weakly anisotropic plates. The accuracy decreased with increasing anisotropy of the plate medium. Analysis has also shown that the reconstruction accuracy is affected by the anisotropy of the defect. This is due to coupling between the velocity and Thomsen parameters in the inversion, which increases the reconstruction error. One strategy to mitigate this is to apply hierarchical iterative inversion strategies on different parameters, which should decrease the ill-posedness of the inversion. These approaches could be tested on the imaging of delaminations in composite plates, where coupling effects between different wavefield parameters are expected due to the anisotropic nature of the defect. One other application area where the method can be extended is the GWT of pipe bends, where the velocity mapping is influenced by the geometric anisotropy of the waveguide.

REFERENCES

[1] E. V. Malyarenko and M. K. Hinders, "Ultrasonic Lamb wave diffraction tomography," *Ultrasonics*, vol. 39, no. 4, pp. 269–281, Jun. 2001.

[2] A. H. Rohde, M. Veidt, L. R. F. Rose, and J. Homer, "A computer simulation study of imaging flexural inhomogeneities using plate-wave diffraction tomography," *Ultrasonics*, vol. 48, no. 1, pp. 6–15, Mar. 2008.

[3] P. Belanger, P. Cawley, and F. Simonetti, "Guided wave diffraction tomography within the born approximation," *IEEE Trans. Ultrason., Ferroelectr., Freq. Control*, vol. 57, no. 6, pp. 1405–1418, Jun. 2010.

[4] P. Huthwaite and F. Simonetti, "High-resolution guided wave tomography," *Wave Motion*, vol. 50, no. 5, pp. 979–993, 2013.

[5] C.-T. Ng, "A two-stage approach for quantitative damage imaging in metallic plates using Lamb waves," *Earthquakes Struct.*, vol. 8, no. 4, pp. 821–841, Apr. 2015.

[6] E. Chan, L. R. F. Rose, and C. H. Wang, "An extended diffraction tomography method for quantifying structural damage using numerical Green's functions," *Ultrasonics*, vol. 59, pp. 1–13, May 2015.

[7] J. Rao, M. Ratassepp, and Z. Fan, "Guided wave tomography based on full waveform inversion," *IEEE Trans. Ultrason., Ferroelectr., Freq. Control*, vol. 63, no. 5, pp. 737–744, May 2016.

[8] A. Volker and J. Bloom, "Experimental results of guided wave travel time tomography," *AIP Conf.*, vol. 1335, pp. 215–222, Jun. 2011.

[9] C. L. Willey, F. Simonetti, P. B. Nagy, and G. Instanes, "Guided wave tomography of pipes with high-order helical modes," *NDT & E Int.*, vol. 65, pp. 8–21, Jul. 2014.

[10] P. Huthwaite and M. Seher, "Robust helical path separation for thickness mapping of pipes by guided wave tomography," *IEEE Trans. Ultrason., Ferroelectr., Freq. Control*, vol. 62, no. 5, pp. 927–938, May 2015.

[11] A. Bulletti, P. Giannelli, M. Calzolai, and L. Capineri, "An integrated acousto/ultrasonic structural health monitoring system for composite pressure vessels," *IEEE Trans. Ultrason., Ferroelectr., Freq. Control*, vol. 63, no. 6, pp. 864–873, Jun. 2016.

[12] A. J. Brath, F. Simonetti, P. B. Nagy, and G. Instanes, "Guided wave tomography of pipe bends," *IEEE Trans. Ultrason., Ferroelectr., Freq. Control*, vol. 64, no. 5, pp. 847–858, May 2017.

[13] A. Segura, P. Lanceleur, J. F. De Belleval, J. M. Gherbezza, and F. Lesage, "Influence of anisotropy for the characterizartion of internal imperfection in pipes by ultrasonic non-destructive testing," *e-J. Nondestruct. Test.*, vol. 14, no. 5, pp. 1–11, 2009.

[14] D. E. Chimenti, "Guided waves in plates and their use in materials characterization," *Appl. Mech. Rev.*, vol. 50, no. 5, pp. 247–284, May 1997.

[15] Z. Su, L. Ye, and Y. Lu, "Guided Lamb waves for identification of damage in composite structures: A review," *J. Sound Vib.*, vol. 295, nos. 3–5, pp. 753–780, Aug. 2006.

[16] O. Putkis, R. P. Dalton, and A. J. Croxford, "The anisotropic propagation of ultrasonic guided waves in composite materials and implications for practical applications," *Ultrasonics*, vol. 65, pp. 390–399, Feb. 2016.

[17] C. A. C. Leckey, K. R. Wheeler, V. N. Hafiychuk, H. Hafiychuk, and D. A. Timuçin, "Simulation of guided-wave ultrasound propagation in composite laminates: Benchmark comparisons of numerical codes and experiment," *Ultrasonics*, vol. 84, pp. 187–200, Mar. 2018.

[18] A. Eremin, E. Glushkov, N. Glushkova, and R. Lammering, "Guided wave time-reversal imaging of macroscopic localized inhomogeneities in anisotropic composites," *Struct. Health Monit.*, vol. 18, pp. 1–17, Nov. 2019.

[19] P. Huthwaite, "Evaluation of inversion approaches for guided wave thickness mapping," *Proc. Roy. Soc. London A, Math., Phys. Eng. Sci.*, vol. 470, no. 2166, 2014, Art. no. 20140063.

[20] J. Rao, M. Ratassepp, and Z. Fan, "Investigation of the reconstruction accuracy of guided wave tomography using full waveform inversion," *J. Sound Vib.*, vol. 400, pp. 317–328, Jul. 2017.

[21] M. Ratassepp, J. Rao, and Z. Fan, "Quantitative imaging of Young's modulus in plates using guided wave tomography," *NDT & E Int.*, vol. 94, pp. 22–30, Mar. 2018.

[22] L. R. F. Rose and C. H. Wang, "Mindlin plate theory for damage detection: Imaging of flexural inhomogeneities," *J. Acoust. Soc. Amer.*, vol. 127, no. 2, pp. 754–763, Feb. 2010.

[23] L. Wang and F. G. Yuan, "Group velocity and characteristic wave curves of Lamb waves in composites: Modeling and experiments," *Compos. Sci. Technol.*, vol. 67, nos. 7–8, pp. 1370–1384, Jun. 2007.

[24] A. J. Brath, F. Simonetti, P. B. Nagy, and G. Instanes, "Acoustic formulation of elastic guided wave propagation and scattering in curved tubular structures," *IEEE Trans. Ultrason., Ferroelectr., Freq. Control*, vol. 61, no. 5, pp. 815–829, May 2014.

[25] A. J. Brath, F. Simonetti, P. B. Nagy, and G. Instanes, "Experimental validation of a fast forward model for guided wave tomography of pipe elbows," *IEEE Trans. Ultrason., Ferroelectr., Freq. Control*, vol. 64, no. 5, pp. 859–871, May 2017.

[26] A. J. Brath and F. Simonetti, "Phased array imaging of complex-geometry composite components," *IEEE Trans. Ultrason., Ferroelectr., Freq. Control*, vol. 64, no. 10, pp. 1573–1582, Oct. 2017.

[27] K. I. Salas and C. E. S. Cesnik, "Guided wave structural health monitoring using CLoVER transducers in composite materials," *Smart Mater. Struct.*, vol. 19, Nov. 2010, Art. no. 015014.

[28] L. Thomsen, "Weak elastic anisotropy," *Geophysics*, vol. 51, no. 10, pp. 1954–1966, Oct. 1986.

[29] I. Tsvankin, "Anisotropic parameters and P-wave velocity for orthorombic media," *Geophysics*, vol. 64, no. 4, pp. 1292–1309, 1997.

[30] Y. Gholami, R. Brossier, S. Operto, A. Ribodetti, and J. Virieux, "Which parameterization is suitable for acoustic vertical transverse isotropic full waveform inversion? Part 1: Sensitivity and trade-off analysis," *Geophysics*, vol. 78, no. 2, pp. R81–R105, Mar. 2013.

[31] T. Alkhalifah and R.-É. Plessix, "A recipe for practical full-waveform inversion in anisotropic media: An analytical parameter resolution study," *Geophysics*, vol. 79, no. 3, pp. R91–R101, May 2014.

[32] Y. Li and T. Alkhalifah, "Multi-parameter reflection waveform inversion for acoustic transversely isotropic media with a vertical symmetry axis," *Geophys. Prospecting*, vol. 68, no. 6, pp. 1878–1892, Jul. 2020.

[33] M. D. Seale and E. I. Madaras, "Lamb wave characterization of the effects of long-term thermal-mechanical aging on composite stiffness," *J. Acoust. Soc. Amer.*, vol. 106, no. 3, pp. 1346–1352, Sep. 1999.

[34] H. Zhou, G. Zhang, and R. Bloor, "An anisotropic acoustic wave equation for modeling and migration in 2D TTI media," in *Proc. 76th Annu. Int. Meeting, SEG, Expanded Abstr.*, 2006, pp. 194–198.

[35] T. Alkhalifah, "An acoustic wave equation for anisotropic media," *Geophysics*, vol. 65, no. 4, pp. 1239–1250, Jul. 2000.

[36] V. Grechka, L. Zhang, and J. W. Rector, "Shear waves in acoustic anisotropic media," *Geophysics*, vol. 69, no. 2, pp. 576–582, Mar. 2004.

[37] S. Operto, J. Virieux, A. Ribodetti, and J. E. Anderson, "Finite-difference frequency-domain modeling of viscoacoustic wave propagation in 2D tilted transversely isotropic (TTI) media," *Geophysics*, vol. 74, no. 5, pp. T75–T95, Sep. 2009.

[38] J. Virieux and S. Operto, "An overview of full-waveform inversion in exploration geophysics," *Geophysics*, vol. 74, no. 6, pp. WCC1–WCC26, Nov. 2009.

[39] B. Hustedt, S. Operto, and J. Virieux, "Mixed-grid and staggered-grid finite-difference methods for frequency-domain acoustic wave modelling," *Geophys. J. Int.*, vol. 157, no. 3, pp. 1269–1296, Jun. 2004.
[40] L. Métivier and R. Brossier, "The SEISCOPE optimization toolbox: A large-scale nonlinear optimization library based on reverse communication," *Geophysics*, vol. 81, no. 2, pp. F1–F15, Mar. 2016.
[41] *ABAQUS/Explicit User's Manual, Version 6.23*, Dassault Syst. Simulia Corp, USA, 2020.
[42] X. Yu, M. Ratassepp, and Z. Fan, "Damage detection in quasi-isotropic composite bends using ultrasonic feature guided waves," *Compos. Sci. Technol.*, vol. 141, pp. 120–129, Mar. 2017.
[43] P. Rajagopal, M. Drozdz, E. A. Skelton, M. J. S. Lowe, and R. V. Craster, "On the use of absorbing layers to simulate the propagation of elastic waves in unbounded isotropic media using commercially available finite element packages," *NDT & E Int.*, vol. 51, pp. 30–40, Oct. 2012.
[44] P. Marguères and F. Meraghni, "Damage induced anisotropy and stiffness reduction evaluation in composite materials using ultrasonic wave transmission," *Compos. A, Appl. Sci. Manuf.*, vol. 45, pp. 134–144, Feb. 2013.
[45] E. Duveneck, P. Milcik, P. M. Bakker, and P. Perkins, "Acoustic VTI wave equations and their application for anisotropic reverse-time migration," in *Proc. 78th Annu. Int. Meeting, SEG, Expanded Abstr.*, 2008, pp. 2186–2190.
[46] B. I. S. Murat, P. Khalili, and P. Fromme, "Scattering of guided waves at delaminations in composite plates," *J. Acoust. Soc. Amer.*, vol. 139, no. 6, pp. 3044–3052, Jun. 2016.
[47] J. E. Anderson, J. R. Krebs, and D. Hinkley, "Source near the free-surface boundary: Pitfalls for elastic finite-difference seismic simulation and multigrid waveform inversion," in *Proc. 70th Annu. Conf. Exhib., EAGE, Extended Abstr.*, 2008, p. WO10.
[48] J. Rao, J. Yang, M. Ratassepp, and Z. Fan, "Multi-parameter reconstruction of velocity and density using ultrasonic tomography based on full waveform inversion," *Ultrasonics*, vol. 101, Feb. 2020, Art. no. 106004.
[49] S. Pant, J. Laliberte, M. Martinez, B. Rocha, and D. Ancrum, "Effects of composite lamina properties on fundamental Lamb wave mode dispersion characteristics," *Compos. Struct.*, vol. 124, pp. 236–252, Jun. 2015.
[50] W. B. Hutchinson, K. Ushioda, and G. Runnsjo, "Anisotropy of tensile behaviour in a duplex stainless steel sheet," *Mater. Sci. Technol.*, vol. 1, pp. 728–731, Sep. 1985.
[51] L. Maio, V. Memmolo, F. Ricci, N. D. Boffa, E. Monaco, and R. Pecora, "Ultrasonic wave propagation in composite laminates by numerical simulation," *Compos. Struct.*, vol. 121, pp. 64–74, Mar. 2015.

Madis Ratassepp received the Ph.D. degree in mechanical engineering from Tallinn University of Technology (TalTech), Tallinn, Estonia, in 2010. His studies focus on ultrasonic-guided wave interaction with defects in plate and pipe structures.

Later, he continued his research as a Postdoctoral Researcher with Nanyang Technological University, Singapore, having a particular interest in ultrasonic guided wave tomography. He is currently a Senior Researcher with TalTech. His research interests include applying ultrasonic-guided waves for structural health monitoring and the inspection of composite materials.

Jing Rao (Member, IEEE) received the Ph.D. degree with focus on quantitative ultrasonic tomography from Nanyang Technological University, Singapore, in 2018.

After completing her Ph.D., she was a Humboldt Research Fellowship holder in the Chair of Computational Modeling and Simulation with the Technical University of Munich, Munich, Germany. She is currently a Lecturer with the School of Engineering and Information Technology, University of New South Wales, Canberra, ACT, Australia. Her research interests include ultrasonicguided wave tomography, structural health monitoring, and quantitative imaging.

Xudong Yu received the Ph.D. degree in aerospace engineering from Nanyang Technological University, Singapore, in 2018, with a focus on ultrasonic nondestructive evaluation (NDE) via structural guided waves.

He continued his research in NDE as a Postdoctoral Research Fellow with Nanyang Technological University, specialized in ultrasonic array imaging of composites. Since 2019, he has been an Associate Professor with the School of Astronautics, Beihang University, Beijing, China. His research interests include ultrasonic NDE, material characterization, and smart materials and structures.

Zheng Fan received the Ph.D. degree from Imperial College London, London, U.K., in 2010, specialized in ultrasonic nondestructive evaluation.

He is currently an Associate Professor with the School of Mechanical and Aerospace Engineering, Nanyang Technological University, Singapore, leading a research team to develop novel techniques for metal and composite inspection, structural health monitoring, and material characterization, by integrating physics and modeling techniques with the development of rapidly exploitable technologies.